

# On Correlated Knowledge Distillation for Monitoring Human Pose with Radios

Shiva Raj Pokhrel, Jonathan Kua, Deol Satish, Phil Williams, Arkady Zaslavsky, Seng W. Loke and Jinho Choi

**Abstract**—In this work, we propose and develop a simple experimental testbed to study the feasibility of a novel idea by coupling radio frequency (RF) sensing technology with Correlated Knowledge Distillation (CKD) theory towards designing lightweight, near real-time and precise human pose monitoring systems. The proposed CKD framework transfers and fuses pose knowledge from a robust “Teacher” model to a parameterized “Student” model, which can be a promising technique for obtaining accurate yet lightweight pose estimates. To ensure its efficacy, we implemented CKD for distilling logits in our integrated Software Defined Radio (SDR)-based experimental setup and investigated the RF-visual signal correlation. Our CKD-RF sensing technique is characterized by two modes – a camera-fed Teacher Class Network (e.g., images, videos) with an SDR-fed Student Class Network (e.g., RF signals). Specifically, our CKD model trains a dual multi-branch teacher and student network by distilling and fusing knowledge bases. The resulting CKD models are then subsequently used to identify the multimodal correlation and teach the student branch in reverse. Instead of simply aggregating their learnings, CKD training comprised multiple parallel transformations with the two domains, i.e., visual images and RF signals. Once trained, our CKD model can efficiently preserve privacy and utilize the multimodal correlated logits from the two different neural networks for estimating poses without using visual signals/video frames (by using only the RF signals).

## I. INTRODUCTION

The advent of the Internet of Things (IoT), Artificial Intelligence (AI)/Machine Learning (ML), and computer vision have significantly advanced the field of human pose estimation and have resulted in many new application domains, such as near real-time fall detection in patient/aged care homes [1], activity sensing [2] and sign language recognition [3]. Most state-of-the-art techniques rely on cameras and, more recently AI-driven computer vision technologies to detect, identify, and react to human pose changes in public/private spaces. These systems can be reliable and provide accurate human pose estimates, but they require expensive equipment and incur high computational costs. In addition, there are data privacy concerns when deploying high-definition visual spectrum cameras where the activity of human subjects is being monitored.

The use of Radio Frequency (RF)-sensing technologies for human pose estimation over the past decade has gained traction and has resulted in significant benefits across a wide range of settings (see [4] and references). For example, people in assisted living facilities can benefit from remote monitoring to ensure their health and safety while maintaining their independence, but privacy is invaded by the use of cameras. RF-sensing could not only monitor diseases of the elderly and disabled but also has great potential for military applications

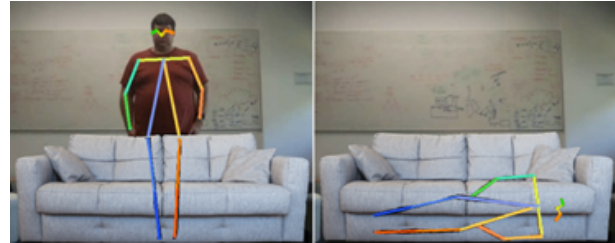


Fig. 1. Motivating example of RF-based pose estimation and tracking through occlusions. Human subjects could be hidden from plain view, as RF signals can penetrate objects.

(e.g., detecting sitting, standing, and lying face up or down) and emergency response such as fires and flood, including others.

Some relevant works directly apply [5]–[10] ML methods for RF-sensing, which have been reported to be strongly biased due to background RF noises and fail to learn helpful information for pose estimates [2], [11]. In a different context, [3] employs ML to demonstrate sign language recognition with RF sensing. However, the researchers in this field have poorly studied the potential of multimodal learning with knowledge fusion/distillation for improving RF-sensing, which is the primary focus of this article.

Figure 1 illustrates a motivating example of using RF signals to detect and track human poses (the subject could be hidden from plain view, as RF signals can penetrate objects). We aim to develop a system to accurately detect and predict human activity without compromising privacy (movement tracking through occlusions) and alleviating the impacts of RF noise. With computational and wireless network resources becoming increasingly cheaper and available, we design an experimental testbed and propose a new technique by coupling RF sensing with knowledge fusion and distillation.

The proposed Correlated Knowledge Distillation (CKD) theory is to drive lightweight, near real-time, and precise human pose estimates. Our CKD-based technique uses “Teacher” and “Student” deep network models to train and implement two modes – a camera-fed Teacher Class Network (e.g., images, videos) with an RF-fed Student Class Network (e.g., RF signals). Our CKD model trains a dual multi-branch teacher and student network and acquires a joint CKD model [12], [13]. The resulting CKD models are subsequently used to identify the multimodal correlation and teach the student branch in reverse [14], [15]. Instead of simply aggregating their learnings, CKD training always seeks to comprise multiple parallel transformations with the two domains, i.e., visual images and RF signals, as feature mapping obtained by feature fusion seldom serves as a good teacher to guide

their training [16]. Once trained, using radio signals generated from a Software Defined Radio (SDR), our CKD model can efficiently preserve privacy and utilize the multimodal correlated logits from the teacher to the student network without using visual signals/video frames.

In this work, we implemented an experimental setup using SDR to realize a hybrid RF and visual camera framework for recognizing human activities while preserving privacy. We developed an in-house, purpose-built experimental testbed to study and investigate the efficacy of our proposed method. We propose a novel CKD-based framework to identify and extrapolate the intricate correlations between RF and visual camera signals. The knowledge/data of correlation between the two signals is then trained using an ML model, which can then be used to drive the RF sensing independent of the visual camera. We implemented a USRP N200 with a UBX 40 USRP Daughterboard and two Omni-directional VERT2450 Antenna. The two antennas serve as a single receiver and single transmitter. We collect data from the SDR and only use its information to estimate pose annotations. The collected (approximate stick figure) data is then used to train (supervised learning) our ML model (using correct pose annotations). This is achieved by using an RGB camera in conjunction with Alphapose. Our experimental results demonstrate the efficacy of our proposed joint CKD-RF sensing approach.

In summary, our contributions to this paper are as follows.

- We develop a purpose-built experimental testbed framework that implements a joint SDR and visual camera-based system for near real-time human pose detection and analytics.
- We design and propose a novel Correlated Knowledge Distillation (CKD) theory to rapidly track the changes in the physical environment by exploiting the multimodal correlation with fusion between RF and visual signals.
- We implement a tractable CKD model for private identification and predictions of human poses without feeding camera images.

The remainder of the paper is organized as follows. Section II provides background information and reviews related work in the area. Section III presents our proposed joint RF and camera-based CKD approach, and Section IV presents the technical setup of our experimental testbed. Section V presents our experimental evaluation details and provides insights from our findings. Section VI identifies key challenges and outlines

future research directions. Section VII concludes the paper.

## II. LITERATURE

In this section, we present the background information and related works pertaining to our findings presented in this paper.

*Software-Defined Radio (SDR):* SDR has recently gained attention in the sensing and communication community due to its unique ability to unify two fundamental technologies, i.e., software and digital radio [17]. Khan et al. [18] shows SDR as a radio communication system enabling the modeling and control of complex RF sensing tasks using a localizing environment to tune the waveforms. There are currently limited research outcomes documented in the literature on using SDR to monitor and identify human activities and/or pose changes.

*Camera-based motion sensing:* The visual camera produces RGB images, and any human pose estimation from these images generally falls under top-down and bottom-up approaches. In a top-down approach, the camera first detects the person from the image, then applies a single-person pose estimator to each person to extract key points [19], [20]. In a bottom-up approach, the camera first detects all the key points in the image first, then does some post-processing to associate the key points [21], [22]. There are several approaches to using multi-person pose estimation from RGB images, for example, Alphapose [19], Yolo [23] and FPN [24]. We exploit Alphapose (which uses a two-stage scheme) as our primary pose supervision resource which can “teach” the mapping from WiFi signals to a person’s pose.

*WiFi-based human activity recognition:* There has been much interest in exploiting wireless signals for locating subjects and monitoring human activities. They can be classified into two categories. The first category utilizes very high frequencies e.g. millimeter wave (mmWave) or terahertz (THz) [25]. It can realistically image the surface of the human body (such as airport security scanners), but it cannot penetrate objects such as walls and furniture. The second category utilizes lower frequencies around a few GHz, thus allowing it to scan through walls and occlusions.

Important related works include crowd counting [5], [6], human identification through physical constraints [7], through-the-wall human detection [8], [26] or through-the-wall activity human activity or gesture recognition [4], [9], [10]. In particular, the work in [27] proposes a state-of-the-art vision model to provide cross-modal supervision. The authors extracted pose information from the visual stream input and use it to guide the training process of the network model. Once the model is sufficiently trained, it will only use wireless signals for pose estimation. Another work in [9] proposed a fully convolutional network to estimate multi-person pose from the collected data and analytics by training with the help of a visual stream from a camera.

*Knowledge Distillation (KD):* CKD proposed in this paper is an enhancement to KD by exploiting a knowledge fusion that extends a “Teacher-Student” approach to transfer knowledge from data/instances derived and collected from separate sources and transfer both instance-level and also the information of correlation between instances [14], [15]. To understand



Fig. 2. Observations without using proposed CKD framework. Right panel: Teacher class original video frame and Alphapose detection. Left panel: Student class CSI trained model and pose detection using standard knowledge distillation

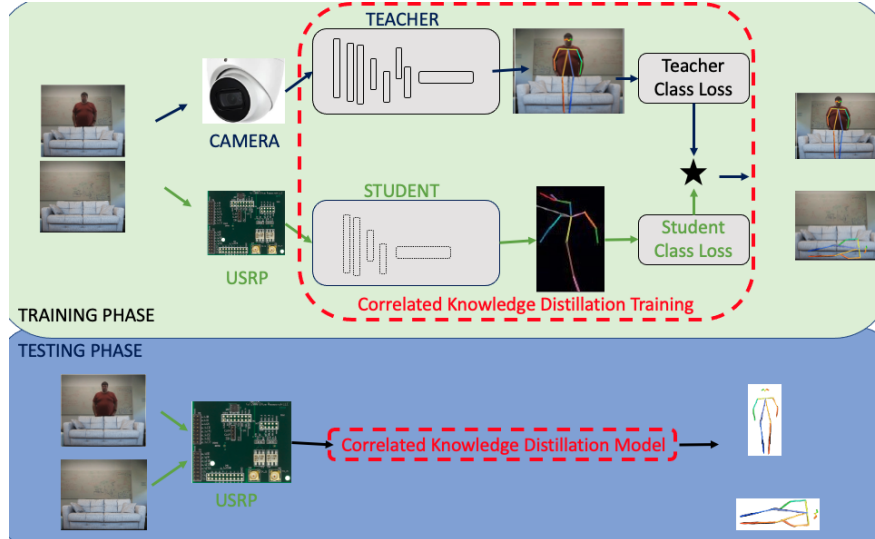


Fig. 3. An abstract view of the proposed correlated knowledge distillation framework. Observe that the classification prediction problem of the standard KD is separated into two levels: (i) a binary prediction for the camera-based teacher class and all RF- sensing based student classes and (ii) a multi-category prediction for each student class. More importantly, we decompose the KD loss into two separate loss components.

this further, we have tested standard KD [12] teacher-student by plugging Alphapose [19] in our experimental testbed. Our observations are shown in Figure 2. We find that the inaccuracy in pose estimates that we can see in the right panel of Figure 2 is due to RF noise and lack of knowledge fusion. In a different context, authors in [14], [15] proposed knowledge distillation (and with fusion [16]), which describes a learning style in which a more extensive teacher Neural Network (NN) guides a student’s NN learning process for numerous assignments. The understanding is passed on to students by such teachers using hidden labels [13] and multiscale fused distillation [16].

To the best of our knowledge, there are currently no existing works in the literature that studies the use of CKD by employing knowledge fusion distillation theory to correlate RF and visual signals (using both SDR and visual camera) and build an integrated deep model to rapidly identify and predict human pose changes. Our work builds on existing literature in RF/WiFi sensing of human activities but extends to using SDR for RF signal generation and using CKD models for data correlation.

### III. CORRELATED RF AND CAMERA-BASED KNOWLEDGE DISTILLATION

In this section, we present the design and technical details of our proposed joint CKD-RF sensing framework and approach for human pose monitoring.

#### A. Proposed Correlated Knowledge Distillation (CKD) model

In our proposed CKD approach, the classification prediction problem of KD is separated into two levels: (i) a binary prediction for the camera-based teacher class and all SDR-based student classes (RF-sensing) and (ii) a multi-category prediction for each student class. As shown in Figure 3, we decompose the KD loss into two components.

i) **Teacher Class Loss:** In camera-based teacher class training, the prediction of the teacher class, denoted by  $\mathcal{T}$ , is provided, but the training of each student class is based only on the transfer of information via binary logit distillation. One plausible explanation is that teacher class KD conveys information on the difficulty of training models with human poses; that is, the information specifies how challenging it is to recognize each pose.

ii) **Student Class Loss:** In Student Class, we consider only the knowledge among student class logits which solely uses the outcomes that are equivalent to or better than those of the conventional KD, demonstrating the critical role of knowledge included in student logits, which may provide insightful hidden information.

We have the following new insights for developing the proposed CKD approach. The potential of logit distillation is constrained for some reasons, leading to uncorrelated results. Furthermore, straightforward early feature fusion with logits does not make a competent teacher direct their own training. We develop a module for correlated feature fusing and distillation, a novel technique for self-distillation. Logits are at more of a semantic and contextual level than deep network features, so intuitively, logit distillation can attain better efficiency than feature distillation. Therefore, we propose decomposing the celebrated KD mechanism towards correlated KD for multimodal learning. Such redesign of the KD approach enables us to investigate the effects of each component separately.

#### B. CKD Theory

The details of the proposed CKD approach are shown as pseudocode in Algorithm 1. We use the following notations to quantify the correlated features classification relevant and irrelevant to the student class,  $\mathcal{S}$ . The classification probability of the logits sample, with  $l_i$  representing the logits of  $i$ -th classification, relevant to the student class is given by  $\mathbf{p} =$

---

**Algorithm 1** Essential details of the Pseudocode of CKD
 

---

```

1  \# temp: the temperature for KD and CKD
2  \# a, b: hyper-parameters
3  class { CKD(Distiller): } {}
4  def (self, student, teacher, cfg):
5      self.ce-loss-weight = cfg.DKD.CE-WEIGHT
6      self.a = cfg.CKD.A
7      self.b = cfg.CKD.B
8      self.tem = cfg.CKD.T
9  def Procedure forward-train(self, csi, frame, target
10 ):
11     logits-student= self.student(csi)
12     with torch.no-grad():
13         logits-teacher = self.teacher(frame)
14 EndProcedure
15 .....
16 def Procedure(LOSS)
17 loss-ce = self.ce-loss-weight * cross-entropy(logits
18 -student, target)
19     loss-CKD = min(epoch / self.warmup, 1.0) *
20     CKDloss(
21         logits-student,
22         logits-teacher,
23         target,
24         self.a,
25         self.b,
26         self.tem
27     )
28 EndProcedure
29 .....
30 def CKDloss(logits-student, logits-teacher, target,
31 a, b, tem):
32     pred-teacher = F.softmax(logits-teacher/tem)
33     pred-student = F.softmax(logits-student/tem)
34     pred-teacher = torch.log(cat-mask(pred-teacher))
35     pred-student = torch.log(cat-mask(pred-student))
36 def TKDloss =(
37     F.NSELoss(pred-student,pred-teacher) * (tem*4)
38 )
39 .....
40 pred-teacher1 = F.log-softmax(logits-teacher/tem -
41 1000.0 * mask(logits, target))
42 pred-student1 = F.log-softmax(logits-student/tem -
43 1000.0 * mask(logits, target))
44 def SKDloss =(
45     F.NSELoss(pred-student1,pred-teacher1) * (tem*4)
46 )
47 return (TKDloss + b * SKDloss)
48 .....
49 def cat-mask(t):
50     compute mask1, mask2
51     t1 = (t * mask1).sum(dim=1, keepdims=True)
52     t2 = (t * mask2).sum(1, keepdims=True)
53     rt = torch.cat([t1, t2])
54     return rt

```

---

$[p_1, p_2, \dots, p_i, \dots, p_N] \in \mathbb{R}^{1 \times N}$ , where  $N$  is the number of classifications and  $p_i$  is the probability of  $i$ -th classification obtained by using the *softmax function*

$$p_i = \frac{\exp(l_i)}{\sum_i^N \exp(l_i)}. \quad (1)$$

Consider  $\bar{\mathbf{p}} = [p_r, p_{\bar{r}}] \in \mathbb{R}^{1 \times 2}$  as the binary probabilities of the relevant classification ( $p_r$ ) and non-relevant classification

( $p_{\bar{r}}$ ), which can be computed as

$$p_r = \frac{\exp(l_r)}{\sum_i^N \exp(l_i)}; \quad (2)$$

$$p_{\bar{r}} = \frac{\sum_{i \neq r}^N \exp(l_i)}{\sum_i^N \exp(l_i)} \quad (3)$$

In addition, without considering the relevant  $r$ -th classification, we quantify the probability  $\hat{p}_i$  as

$$\hat{p}_i = \frac{\exp(l_i)}{\sum_{i \neq r}^N \exp(l_i)} \quad (4)$$

for independently determining the model probabilities

$$\hat{\mathbf{p}} = [\hat{p}_1, \hat{p}_2, \dots, p_{r-1}, p_{r+1}, \dots, p_N] \in \mathbb{R}^{1 \times (N-1)}.$$

Overall, the novelty in the proposed CKD can be viewed in the form of a tractable classification loss process as follows. To enable the student model to learn the logit of the teacher model directly, we compute the loss by applying a Kullback–Leibler (KL) divergence-like measure or the normalized squared error (NSE) between the logit vectors as

$$NSE(\bar{\mathbf{p}}_1, \bar{\mathbf{p}}_2) = \Delta(\bar{\mathbf{p}}_1, \bar{\mathbf{p}}_2) = \frac{\|\log \bar{\mathbf{p}}_1 - \log \bar{\mathbf{p}}_2\|^2}{N}. \quad (5)$$

Observe in (5) that the normalization of the squared error of the CKD estimator is the average of the squared differences between the logarithmic estimated classification probabilities of the teacher and student class. It's a risk function representing the predicted cost of squared deviation, which is never negative, and a value closer to 0 is preferable. Considering that the NSE is the second moment of the difference,  $\Delta(\hat{\mathbf{p}}_1, \hat{\mathbf{p}}_2) = \frac{\|\log \hat{\mathbf{p}}_1 - \log \hat{\mathbf{p}}_2\|^2}{N}$ , we include both the estimator's variance and its bias, to reflect the importance of correlated multimodal learning in the CKD framework.

Using a similar intuition to that of KL-divergence (in the standard KD) for tractability, and using aforementioned analyses, we determine the CKD loss (a joint NSE loss of two classes) as

$$\begin{aligned} CKDloss &= TKDloss + (1 - p_r^T)SKDloss, \\ &= NSE(\bar{\mathbf{p}}^S, \bar{\mathbf{p}}^T) + (1 - p_r^T)NSE(\hat{\mathbf{p}}^S, \hat{\mathbf{p}}^T). \end{aligned} \quad (6)$$

Intuitively,  $TKDloss$  is the feature classification loss,  $SKDloss$  is the model probabilities loss, and  $p_r^T$  is the relevant binary classification probability of the teacher class network. To this end, the standard KD [12] with knowledge fusion facilitates us to look at the distinct effects of TKD and SKD, highlighting the existing approaches' inadequacy in exploiting the underlying correlation and multimodal feature fusion.

### C. Technical setup and design details

To implement the proposed CKD, we extend Alpha-Pose [19] to process the video and annotate the poses with confidence levels and coordinates for each frame accurately. This extension produces a JSON output file that contains person pose coordinates. The number of posing coordinates may differ depending on the dataset and model nevertheless we simply

employ FastPose with the Yolov3 detector and Resnet50 as the backbone for tractability. Unlike AlphaPose [19] generating teacher class model, we extract pose annotations and perform pose estimation from the WiFi Channel State Information (CSI) with learning to correlate with the student class model. However, we find that we cannot accurately determine a person’s pose coordinates simply by analyzing the CSI. See Figure 3 for the details. To ameliorate the shortcoming of such student class training, we have implemented the proposed CKD approach, shown in Algorithm 1, with a camera-oriented teacher model training alongside the WiFi USRP to train the correlated model with videos and CSI.<sup>1</sup> For tractability [19], the underlying Alphapose of the teacher model in our configuration returns 18 key points as shown in Figure 4 or pose coordinates and contributes in determining the corresponding Teacher Class Loss. It is worth noting that these 18 key points

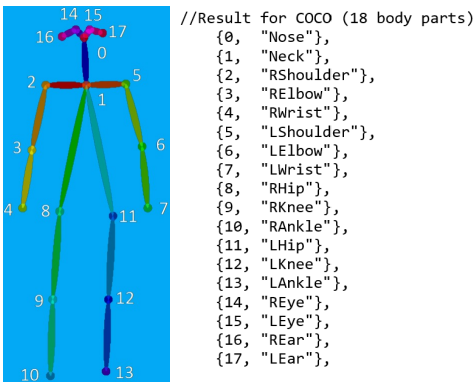


Fig. 4. 18 pose keypoint coordinates.

are computed in the form of a JSON file format with a set of  $\{x_1, y_1, c_1, \dots, x_k, y_k, c_k\}$ .

Our setup and design fully correlate the camera video with WiFi CSI which demonstrates the need for the proposed CKD approach. The WiFi CSI recording system consists of two ends, a sender with three antennas and a USRP with three antennas. When receiving WiFi transmissions, the USRP parses CSI [28] from WiFi signals. The parsed CSI is a tensor of size  $(n \times 53 \times 3 \times 3)$ , where  $n$  is the total number of signals received, 53 is the subcarrier, and the two 3's are the number of sender and receiver antennas respectively. AlphaPose produces  $n$  three-element predictions in the format of  $(x_i, y_i; c_i)$ , where  $n$  is the number of critical points to be estimated,  $x_i$  and  $y_i$  are the coordinates of the  $i$ -th keypoint, and  $c_i$  is the confidence of the aforementioned coordinates. In experiments, we set  $n = 18$ , and use the keypoint configuration as shown in Figure 4.

Assuming that  $I_t$  and  $C_t$  are a pair of synchronized image frames and RF CSI series, respectively,  $t$  denotes the sampling time, the training dataset we generate is denoted by  $D = (I_t, C_t), t \in [1, n]$ . By developing CKD as outlined in Algorithm 1, we trained  $D$  and learnt their correlation. This is the learning mapping rules from the CSI series to

<sup>1</sup>The RGB video is captured using a laptop webcam at 20 frames per second and a 720p resolution, which saves the timestamps for each frame and synchronizes with the corresponding CSI.

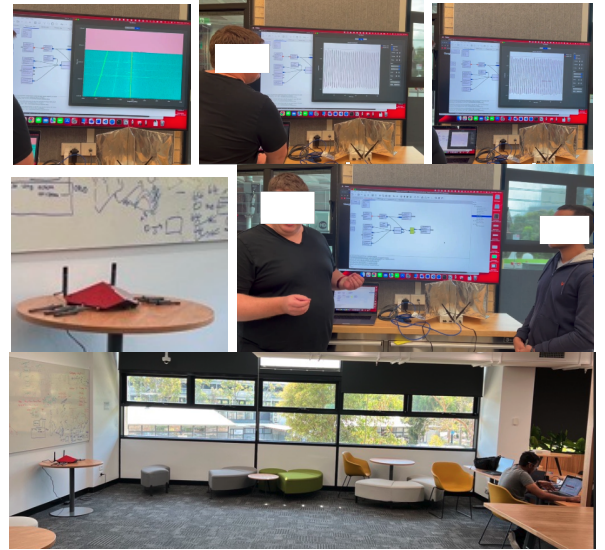


Fig. 5. Images of the testbed setup, videos and RF data collection. The top panel images demonstrate our preliminary approach. The two bottom panels demonstrate our extended testbed setup and data collection.

the frame pose points. The student class network  $\mathcal{S}(\cdot)$  fed with CSI, and the teacher class network fed with AlphaPose,  $\mathcal{T}(\cdot)$ , is the entire CKD framework.  $\mathcal{T}(\cdot)$  accepts  $I_t$  as input, and using the person detector and posture regressor, returns the body keypoint coordinates and confidence,  $(x_t, y_t; c_t)$ , for each pair of  $(I_t, C_t)$ . The outputs are converted into a body pose adjacent matrix, or  $PAM_t$ . 1. Using  $\mathcal{T}(I_t) \rightarrow PAM_t$ , we model how the teacher network teaches  $\mathcal{S}(\cdot)$ , where  $PAM_t$  stands for cross-modality supervision to teach  $\mathcal{S}(\cdot)$ .

In addition to the CKD, we have an encoder, feature generator, and decoder. Encoder upsamples  $C_t$  to proper width and height, suitable for the mainstream convolutional backbone networks and ResNet. Our CSI samples are  $3 \times 3 \times 3$  and the frame RGB is of  $3 \times 244 \times 244$ . Therefore, for CSI, by using eight stacked transposed convolutional layers gradually, we upsampled  $C_t$ . The feature generator learns effective features for estimating a person’s pose coordinates using the upsampled  $C_t$ . To this end, we require a robust feature extractor to generate spatial information from the upsampled  $C_t$ , compared to an image frame, as CSI lacks spatial information of the body key points. We stack four basic ResNet blocks (16 convolutional layers) as feature generators to extract insights (a size of  $300 \times 18 \times 18$ ), which transforms the upsampled  $C_t$  to  $F_t$ .

Our decoder is for shape adaptation and correlation between the learned feature,  $F_t$ , and the supervised output from  $\mathcal{T}(\cdot)$ , the  $PAM_t$ . A body keypoint can be localized in the posture estimation job as two coordinates, namely the  $x$  and  $y$  axes. Therefore, the decoder is built to take  $F_t$  as input and predict adjacency matrix within  $(x, y)$  dimensions resulting in a *predicted pose adjacent matrix*  $\overline{PAM}_t$ . To accomplish this, we have two convolutional layers where the first layer is to release channel-wise information and the second is to reorganize further the spatial information using kernels.

Indeed, the student class deep network predicts a pose

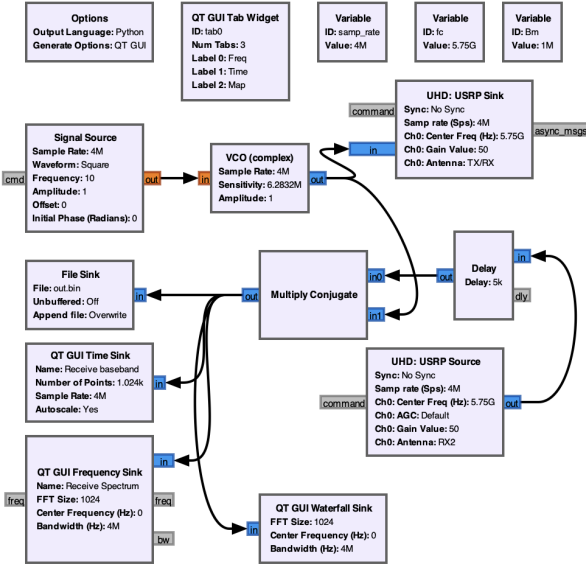


Fig. 6. FMCW Radar design in GNU Radio.

adjacent matrix on each CSI input,  $C_t$ , using the encoder, feature extractor, and decoder. This process is designated as  $S(C_t) \in \overline{PAM}_t$ . Furthermore, with the CKD approach, the  $PAM_t$  resulting from the teacher network is feedback to supervise every predicted  $\overline{PAM}_t$  during the student training.

#### IV. EXPERIMENTAL METHODOLOGY

In this section, we present the setup of our SDR-based testbed and the implementation details of our proposed CKD framework.

Our testbed implements a USRP N200 with a UBX 40 USRP Daughterboard and two Omni-directional VERT2450 Antennas. Using this configuration, we first implemented an FMCW (Frequency-modulated continuous-wave) Radar utilizing the GNU radio, which is a free and open-source radio platform for generating and interpreting radio signals based on C++ and Python. Some of the images of our testbed setup and data collection are shown in the top panel of Figure 5. Figure 6 demonstrates our GNU radio configuration, which is extended with essential insights from PiRadar. The SDR operates at 5.75 GHz and is fed with a saw tooth wave to modulate the carrier. We transmit the modulated carrier and record the reflected signal to detect state variations and predict pose estimates. This preliminary setup provides significant findings however, we are unable to capture body movements from the binary data which reflects very little of the pose changes. Also, the dataset generated is insufficient to feed the deep neural network training and potential knowledge distillation.

With relevant insights from our first experiment, we extend the testbed to capture channel state information (CSI) using the 802.11ac WiFi standard. The images of our extended testbed setup and data collection are also shown in the bottom two panels of Figure 5. The WiFi access points transmit orthogonally modulated beacons containing information about the available WiFi, such as SSID, encryption type, and supported rates. Using the same SDR of our earlier mentioned setup,

we first capture the beacons generated from a different access point in the environment to record the CSI values. We employ PicoScenes [29],<sup>2</sup> to capture our CSI information. In this improved testbed, the USRP N200 is connected to a MacBook Pro-15-inch 2017 with Ubuntu 20.04 to facilitate PicoScenes capturing network traffic over frequency 5220MHz (5Ghz) and channel 44 driven by a Dlink DIR-895L access point. Video frames captured by the MacBook Pro are produced with a timestamp file for synchronization with the CSI.

We position the WiFi access points in our lab to have a clear line of sight from the USRP; 4 and 8 meters is the typical separation between the WiFi access points and the USRP. The project team has followed Deakin University policies and processes for carrying out human subjects' experimentation and data collection. In the two Deakin Lab rooms on the Burwood campus, two authors (Satish and Williams) performed everyday posing tasks for five weeks. Figure 5 shows floor plans and locations for data collection. We use the setup in Figure 5 to simultaneously record CSI samples and videos of 5-7 seconds while the pose actions occur (cf. Figure 3). Each person's 85% of videos and CSI recordings are used to train the networks, while 15% of CSI are used to test the networks. Training and testing have data sizes of 72250 and 12750 videos and CSI samples, respectively. We have received written consent from all participants. The implementation of the CKD framework and sample dataset are publicly available on GitHub.<sup>3</sup>

#### A. Implementation challenges and training details

All convolution and deep networks mentioned earlier are implemented with PyTorch 1.0. They are trained using the Adam optimizer for 20 epochs with an initial learning rate of 0.001. In the teacher-student training of the proposed CKD, we noted that the learning rate decreases by approximately 0.3 near the seventh, tenth, and eighteen epochs. After training, we determine the diagonal elements in the  $\overline{PAM}_t$  as the body keypoint prediction, e.g.,  $x_k^* = \overline{PAM}_{1,k}$  and  $y_k^* = \overline{PAM}_{2,k}$ ,  $k \in [1, 18]$ .

1) *Vanishing Gradient Problem:* We have found that the straightforward implementation and training of the proposed CKD approach suffer from vanishing gradient problems. Therefore, we develop a Residual Block module in PyTorch, which helps in overcoming the vanishing gradient problem prevalent in deep neural network training. In general, the gradients keep decreasing as they are back-propagated through multiple layers leading to the vanishing problem, which creates difficulty for the optimizer to update the weights in the deeper network layers. The developed Residual Block module is for establishing a bypass connection that enables the gradients to skip the levels and directly propagate to the deeper layers, thus alleviating the adverse impacts of such vanishing gradients.

The details of the developed Residual Block are shown in Algorithm 2. It takes as input the number of input channels, the number of output channels, the stride, and an optional

<sup>2</sup>PicoScenes [29] is a middleware tool for capturing the CSI and is compatible with our USRP-based testbed.

<sup>3</sup><https://github.com/Deakin-RF-Sensing>

**Algorithm 2** Important details of the pseudocode of Residual Block developed for ameliorating the vanishing gradients impacts in the proposed CKD approach.

```

1 class ResidualBlock(nn.Module):
2     def __init__(self, in_channels, out_channels,
3         stride=1):
4         super(ResidualBlock, self)...
5         self.bn1 = nn.BatchNorm2d(out_channels)
6         self.relu = nn.ReLU(inplace=True)
7         self.conv1 = conv3x3(in_channels,
8             out_channels, stride)
9         self.conv2 = conv3x3(out_channels,
10             out_channels)
11         self.bn2 = nn.BatchNorm2d(out_channels)
12     def forward(self, x):
13         residual = x
14         out = self.conv1(x)
15         out = self.bn2(self.relu(self.conv2(self.relu(self.bn1(out))))))
16         out += residual
17         out = self.relu(out)
18         return out

```

**Algorithm 3** Important details of the pseudocode of the Extended ResNet Module for the CKD approach.

```

1 class ResNet(nn.Module):
2     def __init__(self, block, layers):
3         super(ResNet, self).__init__()
4         self.in_channels = 150
5         self.conv1 = nn.Sequential(
6             nn.Conv2d(.),
7             nn.BatchNorm2d(.),
8         )
9         self.layer1 = self.make_layer(.)
10        .....
11        self.layer4 = self.make_layer(.)
12        self.decode = nn.Sequential(.),
13        nn.Conv2d(.),
14        )
15    def forward(self, x):
16        x = F.interpolate(.)
17        x = self.layer1(x)
18        .....
19        x = self.decode(x)
20        return x

```

downsample layer for scaling the tensor dimensions. As outlined in Algorithm 2, it has two convolutional layers with a batch normalization layer, a ReLU activation function, and two convolutional layers between each. The residual connection is either the input tensor or the output of the downsample layer.

2) *Revising ResNet for CKD*: We revise and extend the standard ResNet module along the lines of the developed Residual Block discussed earlier. The revision of the ResNet module is to take the developed Residual Block module as input with a list of the number of layers in each block. As shown in Algorithm 3, our ResNet starts with a convolutional neural layer with 150 input and 150 output channels, followed by a batch normalization layer and a ReLU activation. Adopting the *make\_layer* function, it creates four Residual Block, each with increasing input and output channels. Observe in Algorithm 3 that the *make\_layer* is fed with Residual Block, number of input channels, number of blocks, and stride value,

which produces a list of Residual Block modules.<sup>4</sup>

The decoding layer at the end of the developed ResNet has a convolutional layer with 300 input and 64 output channels. It is followed by a batch normalization layer and a ReLU activation function. An input tensor is upsampled using the *F.interpolate* of the ResNet while the output tensor is created by first passing the tensor via the decoding layer.

3) *Interaction of Algorithm 1 with Algorithms 2 and 3*: The interactions of CKD with Algorithms 2 and 3 is shown in Algorithm 4. In our implementation, all other variables, parameters, and constraints such as *Normalized Squared Error (NSE)*, Adam Optimizer, etc. are inherited for the standard ResNet class constructed with a total of 8 Residual Blocks.

**Algorithm 4** Interaction of the components of CKD: Algorithm 1 with Algorithms 2 and 3

```

1 from models.CKD_resnet import ResNet, ResidualBlock,
2     Bottleneck
3 CKD = ResNet(ResidualBlock, [2, 2, 2, 2])
4 resnet = ResNet(ResidualBlock, [3, 4, 6, 3])
5 resnet = ResNet(Bottleneck, [3, 4, 6, 3])
6 CKD = CKD.cuda()
7 criterion_L2 = nn.NSELoss().cuda()
8 optimizer = torch.optim.Adam(CKD.parameters(),
9     lr=learning_rate)
10 scheduler = torch.optim.lr_scheduler.MultiStepLR
11     (optimizer, milestones=[.], gamma=0.5)
12 CKD.train()

```

## V. PERFORMANCE EVALUATION AND ANALYSIS

We have implemented the CKD framework and dataset collected and made it publicly available on GitHub.<sup>5</sup> Small video sequences of 5-7 seconds are captured with the timestamps alongside PicoScenes producing a CSI file containing all WiFi frames. Each frame has a number of features. We extracted the system time with the raw CSI data. This data is then converted/stored as a NumPy array and fed into the CKD along with the matching video frames.

Using a standard KD, we performed the training and testing with the collected dataset for benchmarking. In Figure 7, we can see that the pose estimation using standard KD is entirely inaccurate as the KD Loss framework is unable to capture the distinct difference in the classification loss of the video frame with that of CSI via the student and the teacher network model. In Figure 8, the corresponding variation in the signal strength of the CSI captured by the USRP at four different timestamps under the same posture of the same person is shown in Figure 7. This is due to the adverse impact of RF noise and WiFi traffic fluctuations and demonstrates why the pose estimation directly from RF signals, such as using CSI shown in Figure 7, is erroneous and is highly challenging (without knowledge fusion and correlated distillation from multimodal aspects).

With the proposed CKD approach, we have successfully minimized the training loss considerably over the epoch index,

<sup>4</sup>The first output block of the revised ResNet has the provided number of input channels and output channels, and succeeding blocks have output channels equal to the previous block's input channels.

<sup>5</sup><https://github.com/Deakin-RF-Sensing>

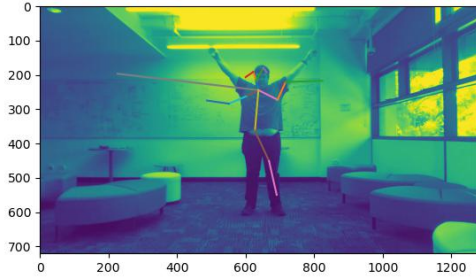


Fig. 7. Testing the student class model using standard KD [13] with test CSI data, pose estimates plotted over the original frame. It is erroneous and demonstrates that only CSI with the KD model cannot quantify the poses accurately.

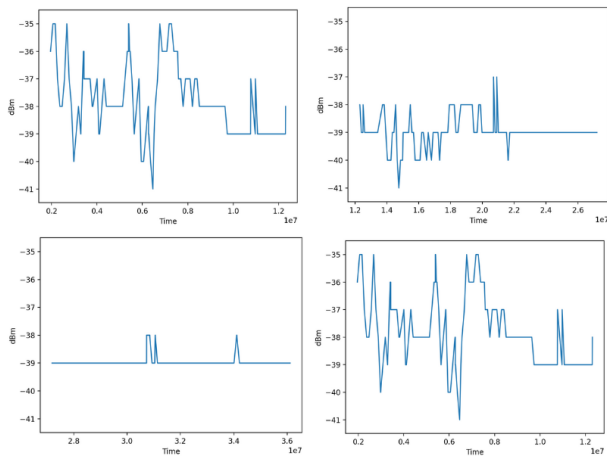


Fig. 8. Signal Strength of CSI captured at USRP for the same pose in the same environment at different timestamps.

as shown in Figure 9. We can see the differences in the evolution of the teacher ( $TKDloss$ ), student ( $SKDloss$ ) and CKD ( $CKDloss$ ) loss over several epochs. This notable improvement (cf.,  $SKDloss \rightarrow CKDloss$ ) considerably increases the accuracy in pose detection, and most pose estimation testing obtained with the trained CKD model is much more accurate. We have shown some examples of our test images with the accuracy of CKD pose estimation in Figure 10.

To understand this further, we compute the MSE over each batch in different training epochs with the proposed CKD. As shown in Figure 11, we found that CKD can exploit correlation for minimizing the loss over increasing batch number considerably. Sample training and testing data can be found in the corresponding GitHub repositories. We have seen practically how the CKD method accelerates learning improves accuracy. Our experiment shows that the CKD model successfully learns a person's posture when the person is relatively stationary and moving slowly but struggles when the person's posture is rapidly changing (as shown in Figure 10).

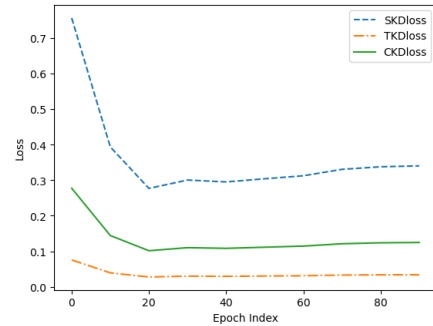


Fig. 9. Evolution of the teacher ( $TKDloss$ ), student ( $SKDloss$ ) and CKD ( $CKDloss$ ) loss over several epochs. The notable improvement (cf.,  $SKDloss \rightarrow CKDloss$ ) considerably increases the accuracy in pose detection, and most pose estimation testing obtained with the trained CKD model is much more accurate.

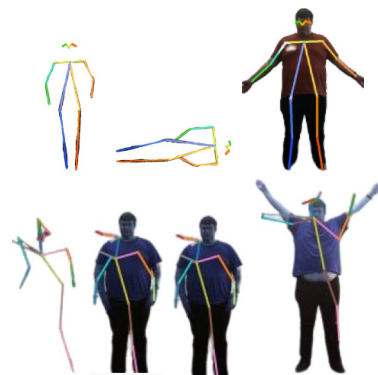


Fig. 10. Testing accuracy of the proposed CKD framework. Top panel: highly accurate pose estimates; bottom panel: relatively low accurate pose estimates; both using the test samples over the same experimental testbed.

## VI. CHALLENGES AND FUTURE DIRECTIONS

Although our findings improved with CKD, the CSI data we collect contains only one dimension because we only employ a single WiFi transmitter and USRP receiver. Therefore, the proposed CKD framework can only accurately extract crucial spatial information by reshaping and upsampling the poor one-dimensional CSI. Future work should expand this study to include scenarios with multiple access points and multiple USRP to test the feasibility of our proposed framework.

There is a great deal of potential in this area and in the ways it may be used. Still, we encountered some challenges (as discussed earlier) during implementation that is now resolved, and we can confidently use the proposed CKD approach. We have identified the following three important directions:

- 1) Our preliminary experiments and studies (along the lines of Figure 8 and 10) with two access points suggest multiple access points and USRP receivers can potentially generate higher accuracy and capture a spatial offset to quantify the dynamic change in CSI efficaciously, which requires extensive experiments in the future.
- 2) We have observed that the volume of WiFi traffic fluctuates over time and can not generate enough RF signals for effective passive listening. Therefore, we need to look for an alternative approach that can more successfully

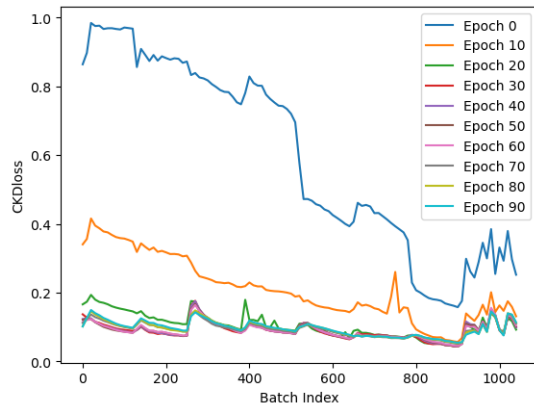


Fig. 11. Comparison of the  $CKDloss$  over each batch index of data in different epochs as observed in our testing setup.

generate enough RF steadily and ameliorate the adverse impacts if RF noise. Such an approach can extend the proposed CKD along the lines of the captured signals and by capturing seamless datasets.

- 3) It appears possible to generate a precise RF signal and monitor it continuously from the access points. An additional module on the top of CKD can assist in understanding and predicting the received RF signal, which can more easily spot deviations.

## VII. CONCLUSIONS

In this work, we developed a Correlated Knowledge Distillation (CKD) system to teach our in-house wireless network, comprising WiFi and USRP, to infer human postures and movements. The CKD system aimed to achieve a hybrid RF and camera framework for privacy-preserving human activity detection using only RF signals. CKD training involved two parallel classification training approaches with images and radios, enabling the fusion and distillation of knowledge. Once trained, the CKD model effectively preserved privacy and leveraged the correlated multimodal logits from the teacher to the student network, eliminating the need for images and video information. Through testing and validation using our SDR-based experimental testbed, we demonstrated the feasibility of the developed CKD framework, highlighting its potential for significant impact in the field. Finally, we also note that the method of training using correlated twin neural networks, where one is a “teacher network” is useful for leveraging pre-trained networks in the absence of (or limited) data.

## REFERENCES

- [1] A. Esteva, K. Chou, S. Yeung, N. Naik, A. Madani, A. Mottaghi, Y. Liu, E. Topol, J. Dean, and R. Socher, “Deep learning-enabled medical computer vision,” *NPJ digital medicine*, vol. 4, no. 1, p. 5, 2021.
- [2] W. Taylor *et al.*, “An implementation of real-time activity sensing using Wi-Fi: Identifying optimal machine-learning techniques for performance evaluation,” *IEEE Sensors Journal*, vol. 22, no. 21, pp. 21127–21134, 2022.
- [3] S. Z. Gurbuz, A. C. Gurbuz, E. A. Malaia, D. J. Griffin, C. S. Crawford, M. M. Rahman, E. Kurtoglu, R. Aksu, T. Macks, and R. Mdrafi, “American sign language recognition using RF sensing,” *IEEE Sensors Journal*, vol. 21, no. 3, pp. 3763–3775, 2021.
- [4] S. Yue, Y. Yang, H. Wang, H. Rahul, and D. Katabi, “Bodycompass: Monitoring sleep posture with wireless signals,” *Proceedings of the ACM on Interactive, Mobile, Wearable and Ubiquitous Technologies*, vol. 4, no. 2, pp. 1–25, 2020.
- [5] S. Depatla and Y. Mostofi, “Crowd counting through walls using WiFi,” in *2018 IEEE international conference on pervasive computing and communications (PerCom)*, pp. 1–10, IEEE, 2018.
- [6] A. Hanif, M. Iqbal, and F. Munir, “Wispy: Through-wall movement sensing and person counting using commodity WiFi signals,” in *IEEE Sensors*, pp. 1–4, IEEE, 2018.
- [7] L. Cheng and J. Wang, “Walls have no ears: A non-intrusive WiFi-based user identification system for mobile devices,” *IEEE/ACM Transactions on Networking*, vol. 27, no. 1, pp. 245–257, 2019.
- [8] H. Sun, L. G. Chia, and S. G. Razul, “Through-wall human sensing with WiFi passive radar,” *IEEE Transactions on Aerospace and Electronic Systems*, vol. 57, no. 4, pp. 2135–2148, 2021.
- [9] F. Wang, J. Feng, Y. Zhao, X. Zhang, S. Zhang, and J. Han, “Joint activity recognition and indoor localization with WiFi fingerprints,” *IEEE Access*, vol. 7, pp. 80058–80068, 2019.
- [10] H. Abdelnasser, K. Harras, and M. Youssef, “A ubiquitous WiFi-based fine-grained gesture recognition system,” *IEEE Transactions on Mobile Computing*, vol. 18, no. 11, pp. 2474–2487, 2018.
- [11] T. Li *et al.*, “Unsupervised learning for human sensing using radio signals,” in *Proceedings of the IEEE/CVF Winter Conference on Applications of Computer Vision*, pp. 3288–3297, 2022.
- [12] G. Hinton, O. Vinyals, and J. Dean, “Distilling the knowledge in a neural network,” *stat*, vol. 1050, p. 9, 2015.
- [13] Z. Li, J. Ye, M. Song, Y. Huang, and Z. Pan, “Online knowledge distillation for efficient pose estimation,” in *Proceedings of the IEEE/CVF International Conference on Computer Vision*, pp. 11740–11750, 2021.
- [14] B. Peng, X. Jin, J. Liu, D. Li, Y. Wu, Y. Liu, S. Zhou, and Z. Zhang, “Correlation congruence for knowledge distillation,” in *Proceedings of the IEEE/CVF International Conference on Computer Vision*, pp. 5007–5016, 2019.
- [15] X. Li, J. Wu, H. Fang, Y. Liao, F. Wang, and C. Qian, “Local correlation consistency for knowledge distillation,” in *Computer Vision—ECCV 2020: 16th European Conference, Glasgow, UK, August 23–28, 2020, Proceedings, Part XII*, pp. 18–33, Springer, 2020.
- [16] L. Li *et al.*, “Knowledge fusion distillation: Improving distillation with multi-scale attention mechanisms,” *Neural Processing Letters*, pp. 1–16, 2023.
- [17] W. H. W. Tuttlebee, *Software Defined Radio*. John Wiley & Sons, 2002.
- [18] M. Z. Khan, A. Taha, W. Taylor, M. A. Imran, and Q. H. Abbasi, “Non-invasive localization using software-defined radios,” *IEEE Sensors Journal*, vol. 22, no. 9, pp. 9018–9026, 2022.
- [19] H.-S. Fang, S. Xie, Y.-W. Tai, and C. Lu, “Rmpe: Regional multi-person pose estimation,” in *Proceedings of the IEEE international conference on computer vision*, pp. 2334–2343, 2017.
- [20] G. Papandreou, T. Zhu, N. Kanazawa, A. Toshev, J. Tompson, C. Bregler, and K. Murphy, “Towards accurate multi-person pose estimation in the wild,” in *Proceedings of the IEEE conference on computer vision and pattern recognition*, pp. 4903–4911, 2017.
- [21] L. Pishchulin, E. Insafutdinov, S. Tang, B. Andres, M. Andriluka, P. V. Gehler, and B. Schiele, “Deepcut: Joint subset partition and labeling for multi person pose estimation,” in *Proceedings of the IEEE conference on computer vision and pattern recognition*, pp. 4929–4937, 2016.
- [22] Z. Cao, T. Simon, S.-E. Wei, and Y. Sheikh, “Realtime multi-person 2d pose estimation using part affinity fields,” in *Proceedings of the IEEE conference on computer vision and pattern recognition*, pp. 7291–7299, 2017.
- [23] J. Redmon, S. Divvala, R. Girshick, and A. Farhadi, “You only look once: Unified, real-time object detection,” in *Proceedings of the IEEE conference on computer vision and pattern recognition*, pp. 779–788, 2016.
- [24] T.-Y. Lin, P. Dollár, R. Girshick, K. He, B. Hariharan, and S. Belongie, “Feature pyramid networks for object detection,” in *Proceedings of the IEEE conference on computer vision and pattern recognition*, pp. 2117–2125, 2017.
- [25] Y. Zhu, Y. Zhu, B. Y. Zhao, and H. Zheng, “Reusing 60ghz radios for mobile radar imaging,” in *Proceedings of the 21st Annual International Conference on Mobile Computing and Networking*, pp. 103–116, 2015.
- [26] M. Zhao, Y. Liu, A. Raghu, T. Li, H. Zhao, A. Torralba, and D. Katabi, “Through-wall human mesh recovery using radio signals,” in *Proceedings of the IEEE/CVF International Conference on Computer Vision*, pp. 10113–10122, 2019.

- [27] M. Zhao, T. Li, M. Abu Alsheikh, Y. Tian, H. Zhao, A. Torralba, and D. Katabi, "Through-wall human pose estimation using radio signals," in *Proceedings of the IEEE Conference on Computer Vision and Pattern Recognition*, pp. 7356–7365, 2018.
- [28] D. Halperin, W. Hu, A. Sheth, and D. Wetherall, "Tool release: Gathering 802.11 n traces with channel state information," *ACM SIGCOMM computer communication review*, vol. 41, no. 1, pp. 53–53, 2011.
- [29] Z. Jiang, T. H. Luan, X. Ren, D. Lv, H. Hao, J. Wang, K. Zhao, W. Xi, Y. Xu, and R. Li, "Eliminating the barriers: Demystifying wi-fi baseband design and introducing the picoscenes wi-fi sensing platform," *IEEE Internet of Things Journal*, vol. 9, no. 6, pp. 4476–4496, 2022.